PERGAMON

International Journal of Solids and Structures 36 (1999) 5029–5055

INTERNATIONAL JOURNAL OF SOLIDS and STRUCTURES

www.elsevier.com/locate/ijsolstr

A void–crack nucleation model for ductile metals

Mark F. Horstemeyer[a,*], Arun M. Gokhale[b]

[a] *Sandia National Laboratories, P.O. Box 969, Livermore, CA 94551-0969, U.S.A.*
[b] *Georgia Institute of Technology, Atlanta, GA 30332-0405, U.S.A.*

Received 14 January 1998; in revised form 23 July 1998; accepted 2 August 1998

Abstract

A phenomenological void–crack nucleation model for ductile metals with second phases is described which is motivated from fracture mechanics and microscale physical observations. The void–crack nucleation model is a function of the fracture toughness of the aggregate material, length scale parameter (taken to be the average size of the second phase particles in the examples shown in this writing), the volume fraction of the second phase, strain level, and stress state. These parameters are varied to explore their effects upon the nucleation and damage rates. Examples of correlating the void–crack nucleation model to tension data in the literature illustrate the utility of the model for several ductile metals. Furthermore, compression, tension, and torsion experiments on a cast Al–Si–Mg alloy were conducted to determine void–crack nucleation rates under different loading conditions. The nucleation model was then correlated to the cast Al–Si–Mg data as well.

1. Introduction

Ductile fracture of engineering alloys is a primary mode of material failure occurring when pores or voids nucleate, grow, and coalesce. In this paper, a new void nucleation model is proposed to more accurately determine damage evolution of ductile metals for use in finite element simulations. We use the term void nucleation instead of crack initiation because our applications relate to ductile metals. We recognize that some researchers use the terminology of a crack rather than a void to describe a defect in a material. Nevertheless, whether a crack-like void or void-like crack occurs, we employ the term void in this setting. Section 2 summarizes the damage framework. Section 3 describes the development of the nucleation model from the basis of fracture mechanics. In Section 4, the void nucleation model parameters are studied in terms of their influence on the nucleation rate and total damage rate. Section 5 includes some examples of the model correlated to literature data of several ductile metals. Also included in this section are void nucleation data

* Corresponding author. Fax: +1 510 294 3470; e-mail: mfhorst@sandia.gov

0020-7683/99/$ - see front matter
PII: S0020-7683(98)00239-X

from compression, tension, and torsion of a cast Al–Si–Mg alloy that were performed to distinguish between stress states. The void nucleation model was correlated to this data as well.

2. Damage description

The damage state of a material can be described in terms of void nucleation and void growth. Let N equal the total number of voids in a representative continuum volume V_0 of material in the initial state (State 0), and let η be the number of voids per unit volume of the material; hence, $\eta = N/V_0$. The average void volume then is

$$v_v = 1/N \sum_{i=1}^{N} v_i$$

where v_i is the void volume from each particle that has nucleated a void. In terms of a rate equation for v_v, one can use void growth models (e.g., McClintock, 1968). Thus the volume of voids is given by

$$V_v = \eta V_0 v_v \tag{1}$$

Damage, ϕ, can be defined as the ratio of volume of an element in its current state to its volume in the initial reference state. As such, the definition of damage can be described by the following equation

$$\phi = \frac{V_v}{V_1} \tag{2}$$

where V_1 is the updated state from the initial configuration $V_1 = V_v + V_0$. Combining eqns (1) and (2), the void volume fraction, ϕ, described by Davison et al. (1977) can be written as

$$\phi = \frac{\eta V_0 v_v}{V_0 + \eta V_0 v_v} = \frac{\eta v_v}{1 + \eta v_v} \tag{3}$$

The damage formulation is shown conceptually in Fig. 1. The number density of voids can change and growth of voids can occur independently or simultaneously. This framework is illustrated by the schematic in Fig. 2 when examining the limiting cases. One void can exist that is growing or many voids can nucleate at the expense of void growth. A typical void growth rule is assumed to have an initial void embryo of a size determined by optical micrographs or some other method. As such, the growth rule applies to voids that are already present and those that are nucleating. These two types of voids would experience the same void growth rule in the damage analysis. Because the void growth rule is initialized with a positive volume, the nucleated void volume is assumed to incur this same initialization volume. Perhaps the most realistic embryo size for the newly nucleated site is the size of the second phase particle. The framework conceivably allows for this initialization as well. For materials with second phases and pre-existing voids, one would anticipate that the average size of the second phase and average size of the pre-existing voids is different. Finally, nucleation is assumed to occur by decohesion of the particle/matrix interface or by particle fracture, but more than one void can be nucleated at a given particle.

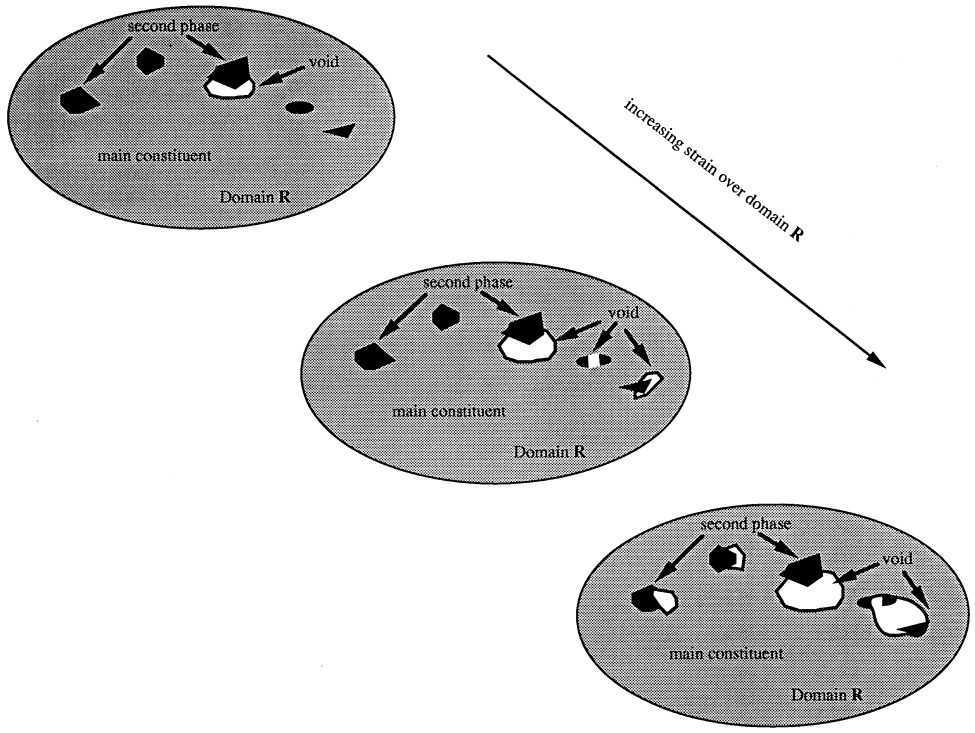

Fig. 1. Schematic of fictitious material with increasing nucleation density and void growth in which the model framework conceptually comprises.

Damage in the context of numerical analysis has also been defined by other methods (cf Barbee et al., 1972; Gurson, 1977a, b; Chen et al., 1984; Tvergaard, 1990; Leblond et al., 1995; Marin, 1993). These methods are characterized by an additive decomposition of damage into nucleation and growth terms instead of a multiplicative decomposition as presented in this writing. Further discussion of these differences can be found in Horstemeyer et al. (1998).

3. Nucleation model derivation

In this section, the model derivation for void nucleation will be explained with a very short discussion on void growth and void coalescence. In general, voids nucleate at sites of local microscale stress raisers. The majority of voids nucleate at inclusions, precipitates, and other second phases of ductile metals (Palmer and Smith, 1967; Gurland, 1972; Cox and Low, 1974; Hahn and Rosenfield, 1975). Voids can also nucleate at the intersection of slip bands (Gysler et al., 1974; Asaro, 1979), at grain boundaries (Nieh and Nix, 1980), at twin boundaries (Lu et al., in press), and at vacancy clusters (Wilsdorf, 1983). In this writing, a void nucleation model is introduced based from microstructural analysis related to second phase particles.

The formulation presented in this paper is consistent with the thermodynamic framework that

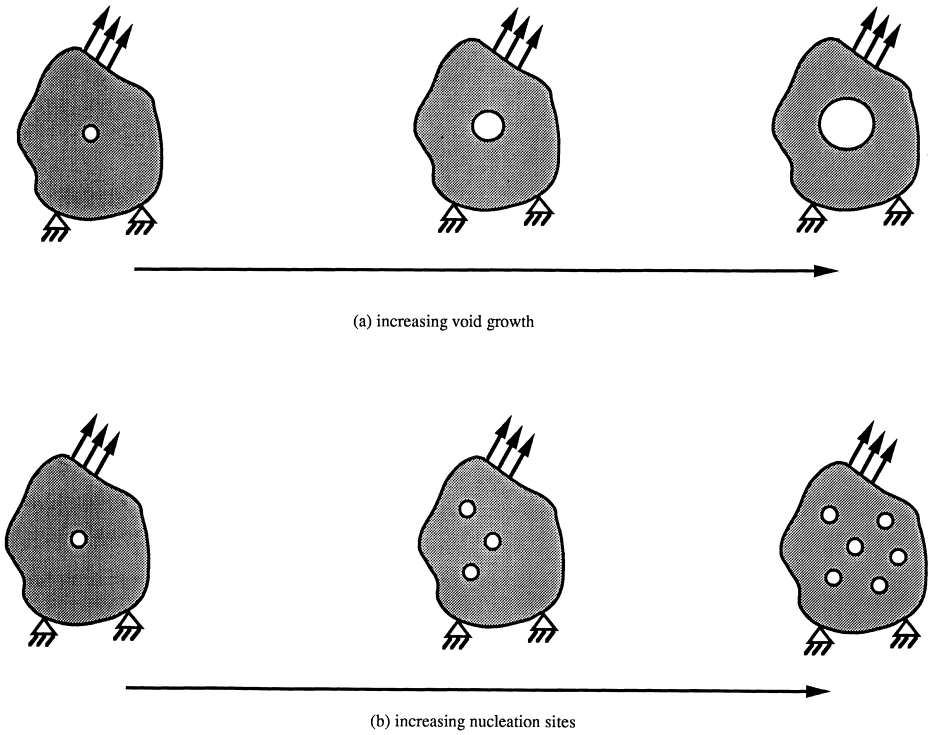

Fig. 2. The model framework encompasses the limiting cases shown by a single void growing in (a) and by damage accumulation from just nucleation in (b).

constrains state damage parameters (Coleman and Gurtin, 1967). Because this development is cast in a macroscale continuum damage mechanics formulation, phenomenological notions are recognized to play a role; however, lower length scale physical observations are used to motivate the void nucleation evolution equation. The thermodynamic restrictions are elucidated further in Horstemeyer et al. (1998).

The void nucleation evolution equation is a function of a length scale parameter (chosen to be the mean size of inclusions for this study), volume fraction of second phase materials, stress state (invariants of stress), strain rate, and fracture toughness. Nucleation models have been proposed in the past in trying to address some of these attributes (cf Gurland and Plateau, 1963; Ashby, 1966; Rosenfield, 1968; Barbee et al. 1972; Argon et al. 1975; Raj and Ashby, 1975; Gurson, 1977a, b; Needleman and Rice, 1978; Goods and Brown, 1979; Tvergaard, 1982a; Saje et al., 1982; Hirth and Nix, 1985), but none include all of the features mentioned above that have been shown to influence the damage state.

In short, the void nucleation model will be motivated from fracture toughness and extended into a rate form in a phenomenological manner. A complicated stress function will be added to supplant the yield stress. A length scale parameter is added to incorporate a size effect within the model. Finally, the volume fraction of the second phase is added in a manner that reflects experimental observations.

Void-crack nucleation truly starts at the atomic level where dislocations are emitted from the crack tip. The void–crack then grows to a point where it can be empirically observed by optical methods. In the present phenomenological formulation, a void–crack is observed empirically by optical methods and the atomistic level of void–crack is not considered. Because of this assumption for the initial embryo size, we first consider the Irwin (1958) fracture mechanics equation, which accounts for a small amount of plasticity near an already formed void-crack. The stress intensity from the Irwin equation is given by

$$K_I = \sigma_y \sqrt{2r_p}\lambda(w) \tag{4}$$

where σ_y is the yield stress, r_p is the plastic zone size, and $\lambda(w)$ is a function based on the geometry of a specimen. When the stress intensity reaches a critical value, the fracture toughness is defined. In generalizing eqn (4) for the dynamic fracture case, we get

$$K_I = K_{IC} = f(\sigma)g(d)\lambda(w)h(\text{rate}) \tag{5}$$

where $f(\sigma)$ is not just limited to a scalar yield strength but can be a flow stress function that distinguishes stress state behavior based upon the three stress invariants. Instead of r_p, we propose $g(d)$ a function related to size scale parameter. And for $\lambda(w)$, material constants will be introduced that will account for fracture arising from the geometry. h(rate) is a function related to strain rate. Cox and Low (1974) and Maloney and Garrison (1989) observed that a resistance to void nucleation promotes higher fracture toughness. Hence, the more nucleation that occurs, the less tough the material. No mathematical form was given for this relation, but a simple function such as that following can be inferred from the qualitative statements made in those papers,

$$h(\text{rate}) = \frac{\eta \|\underline{\dot{\varepsilon}}\|}{\dot{\eta}} \tag{6}$$

By introducing this function, the strain rate, $\underline{\dot{\varepsilon}}$, would be included into the fracture criterion. Kanninen and Popelar (1985) summarized several works describing a nonlinear rate effect on fracture that were dependent on assumptions related to elasticity and the geometry of the specimen. Brickstad (1983) employed Perzyna's viscoplastic model with experimental data that eliminated the geometry effects and the nonlinear effects. Research to quantify fracture rate effects as a function of void nucleation is still an open area. Nevertheless, we assume the form expressed by eqn (6) with an openness to modification when more data is available.

The simplest representation for the flow stress function is a rate independent yield function. The J_2 theory yield function is probably the most widely used form for inelasticity, where J_2 is the second invariant of deviatoric stress defined by

$$J_2 = \tfrac{1}{2} S_{ij} S_{ij}. \tag{7}$$

The second rank stress deviator is defined by $S_{ij} = \sigma_{ij} - \sigma_{\text{hydro}}\delta_{ij}$, where $\sigma_{\text{hydro}} = 1/3\sigma_{kk}$. The stress function that we will employ in equation (5) is introduced as

$$f(\sigma) = z(I_1, J_2, J_3), \tag{8}$$

where

$$z(I_1, J_2, J_3) = a\left[\frac{4}{27} - \frac{J_3^2}{J_2^3}\right] + b\frac{J_3}{J_2^{3/2}} + c\left\|\frac{I_1}{\sqrt{J_2}}\right\|, \tag{9}$$

and

$$I_1 = \sigma_{ii}, J_3 = \tfrac{1}{3}S_{ij}S_{ij}S_{ij}. \tag{10}$$

The material constants a, b, and c are determined from different stress states. This complicated form is elucidated further in the next section, but the reader should know that the motivation for including these particular stress invariant forms in eqn (9) is to allow for the void nucleation model to distinguish between tension, compression, and torsion (cf Miller and McDowell, 1992).

The size-related parameter is given by

$$g(d) = \sqrt{d}, \tag{11}$$

where d is a length scale parameter determined by the most important length scale feature that drives the void nucleation. For example, it can be assumed to be the average particle size of the second phase or the distance between particles.

We can now solve for the void nucleation rate as a function of fracture toughness by substituting eqns (6), (8), (9), and (11) into eqn (5) and then solving for the void nucleation rate,

$$\dot{\eta} = \frac{\|\underline{\dot{\varepsilon}}\| d^{1/2}}{K_{IC}}\eta\left\{a\left[\frac{4}{27} - \frac{J_3^2}{J_2^3}\right] + b\frac{J_3}{J_2^{3/2}} + c\left\|\frac{I_1}{\sqrt{J_2}}\right\|\right\}, \tag{12}$$

yielding a nondimensionalized function.

Fracture toughness can be influenced by the initial volume fraction of inclusions as Gangalee and Gurland (1967) observed for aluminum alloys, Hahn et al. (1968) for several steel and aluminum alloys, and Moody et al. (1993) for powder-processed titanium alloys. Hence, the initial volume fraction of inclusions is included in the nucleation rate from Gangalee and Gurland (1967) form as

$$\dot{\eta} = \frac{\|\underline{\dot{\varepsilon}}\| d^{1/2}}{K_{IC} f^{1/3}}\eta\left\{a\left[\frac{4}{27} - \frac{J_3^2}{J_2^3}\right] + b\frac{J_3}{J_2^{3/2}} + c\left\|\frac{I_1}{\sqrt{J_2}}\right\|\right\}, \tag{13}$$

Gangalee and Gurland (1967) showed that the $d^{1/2}/f^{1/3}$ ratio is useful over a broad range of particle volume fractions and sizes for aluminum–silicon alloys. As a particle is fractured or debonded from the matrix material, its capacity to hold strength is reduced and hence it would probably not fracture or debond again as the energy is being released to drive void growth. Because of this local stress redistribution, this particle is not capable of creating a void again, hence the volume fraction of the second phase that is capable of creating a void is reduced. This change would probably be negligible though in practical applications, so the volume fraction of second phase particles, f, can be approximated by the initial volume fraction of second phases.

The inclusion of the volume fraction in the denominator is counter intuitive at first glance. One might think that the more volume of a second phase present, the more chances exist of nucleating particles. However, the opposite has been experimentally observed (cf Gangalee and Gurland,

1967; Hahn et al., 1968; Moody et al., 1993). This is due to the fact that the distribution of particle spacing is inherently included in the diameter over volume ratio.

The void nucleation rate, denoted by eqn (13), is a function of stress state, strain rate, fracture toughness, average size of second phase particles (which are assumed to be round), and initial volume fraction of second phase particles. Rice and Johnson (1970) showed that for small second phase particles, the fracture toughness scales linearly with particle spacing; hence, particle spacing effects are effectively included in this model.

Equation (13) readily yields the following qualitative trends for the void nucleation rate. As the fracture toughness and initial void volume fraction increase, the nucleation rate decreases. As the stress, strain rate, and particle size increase, the void nucleation rate increases.

When integrating this evolution equation over time, a constant strain rate, fracture toughness, particle size, and particle volume is assumed resulting in the following form,

$$\eta(t) = C_{\text{coeff}} \exp\left(\frac{\varepsilon(t) d^{1/2}}{K_{IC} f^{1/3}} \left\{ a\left[\frac{4}{27} - \frac{J_3^2}{J_2^3}\right] + b\frac{J_3}{J_2^{3/2}} + c\left\| \frac{I_1}{\sqrt{J_2}} \right\| \right\}\right), \tag{14}$$

where $\varepsilon(t)$ is the strain magnitude at time, t, and C_{coeff} is material constant that scales the response as a function of initial conditions since it is equal to a constant times η_0, in which η_0 is the lower limit of the integration signifying an initial void nucleation level.

The damage evolution used from eqn (3) requires a void growth rule with the void nucleation equation. A simple void growth rule is introduced based on the stress triaxiality (hydrostatic stress over the effective stress) so that trends can be observed about the damage state when parameters in the void nucleation model are changed. The simple void growth rule is given by

$$\dot{v}_v = \sinh\left(0.001 \frac{\sigma_{\text{hydro}}}{\sigma_{\text{eff}}}\right), \tag{15}$$

where $\sigma_{\text{eff}} = \sqrt{3J_2}$. We recognize that many more complicated void growth rules are available but the focus of this research as not on void growth per se; hence, this simple one was used. The initial porosity level was chosen to be 0.0001 unless otherwise specified.

No specific void coalescence rule was included in this modeling framework so as to model the void sheet mechanism. Again, we focus in this writing on the void nucleation model, but for the sake of completeness recognize that void coalescence can play a major role in final failure of a material.

The nucleation model was developed for an elastic–plastic material. The nucleation model can fit several plasticity modeling frameworks (cf Bammann, 1988). For sake of brevity, a simple elastic–plastic rod with bi-linear hardening was used to model A356 cast aluminum in a uniaxial stress state in the following analyses unless otherwise specified. The loads were applied in tension except for the case when different boundary conditions were studied.

4. Parametric study

In the next section, we elucidate each of the void nucleation parameters employed in eqn (14) by examining ranges of the parameters. In doing so, we analyze a pseudo-material that has

Table 1
The parameters used for various loading conditions

Parameters	Nominal values
d (μm)	4
f	0.07
K_{1C} (MPa-m**0.5)	46.0
C_{coeff}	5.0
a (MPa)	3e5
b (MPa)	0
c (MPa)	5e4
$\dot{\varepsilon}_{11}$ (s^{-1})	0.1

representative values for real materials. Table 1 summarizes the parameters used except where the parameter was examined for its sensitivity. The strain rate, $\underline{\dot{\varepsilon}}$, is given by the only prescribed component for uniaxial tension as $\dot{\underline{\varepsilon}}_{11}$.

4.1. *Length scale parameter*, d

The length scale parameter chosen for this initial study is that of the average size of the second phase particles. The average particle size of second phases can vary significantly depending on the material and processing method. For materials such as powder processed titanium alloys (cf Moody et al., 1993), the second phase particle sizes can range from 1–3 μm in diameter. For A356 cast aluminum the second phase silicon can range from 3–10 μm (cf Gangalee and Gurland, 1967). For the cast Al–Si–Mg alloy used in this study to analyze the different loading conditions, the silicon particle size ranged from 4–70 μm.

Figure 3(a) shows the density of voids nucleated per unit volume vs strain level for varying particle size. The trends agree with the observations that void nucleation occurs first at larger particles for a number of different materials (cf Gurland, 1972; Cox and Low, 1974; Hahn and Rosenfield, 1975). Figure 3(a) illustrates a nonlinear behavior for the nucleation rate. Figure 3(b) shows the increased accumulation of total damage from void nucleation and growth with the increases in particle size as a function of strain.

4.2. *Particle volume fraction*, f

Volume fractions of second phases in composites can be widespread depending on the material and processing method. For materials such as powder processed titanium alloys (cf Moody et al., 1993), the second phase can range from 0.2–7% by volume. For A356 cast aluminum the second phase silicon can range from 1–13% (cf Gangalee and Gurland, 1967) by volume. Some metal matrix composites can have up to 30% by volume fraction of second phases.

The initial volume fraction of second phase is included in the void nucleation rate equation with a power to the one-third because of observations made by Gangalee and Gurland (1967). For

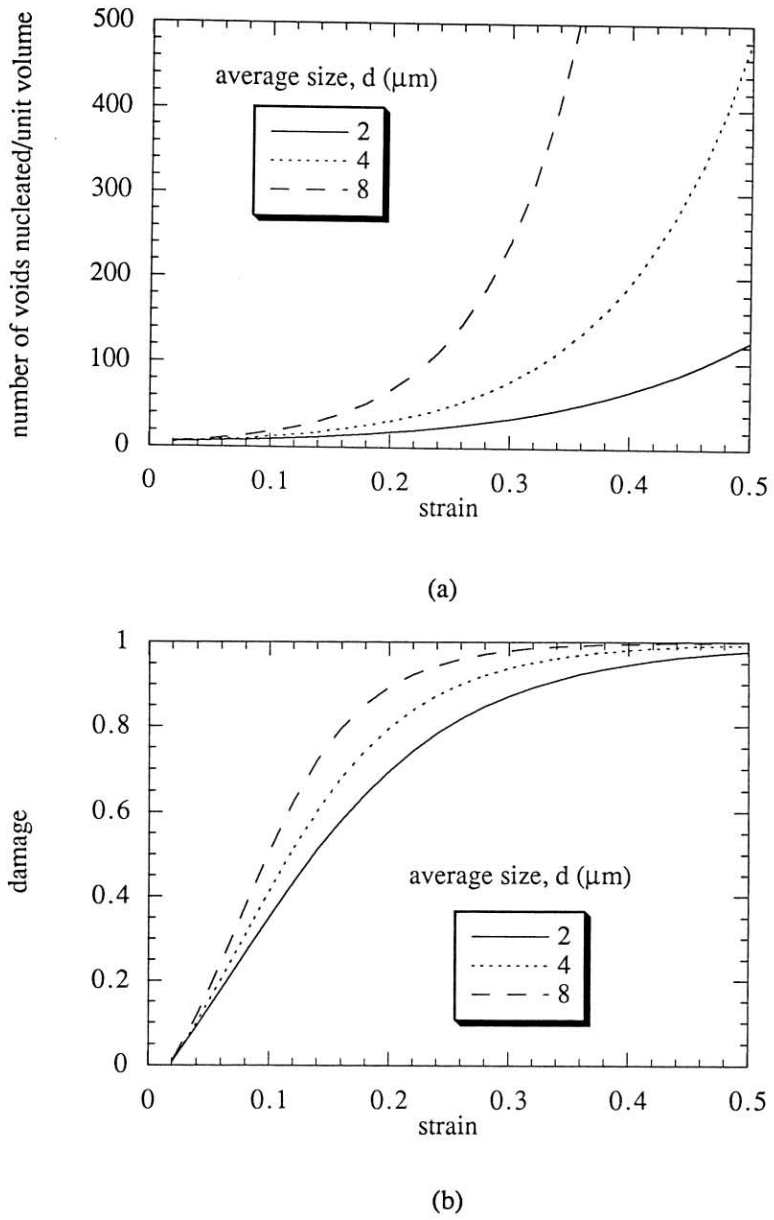

Fig. 3. (a) Nucleation per unit volume vs strain and (b) damage vs strain under uniaxial tension showing the increase in number of voids and total damage as the particle size increases.

silicon particles embedded in aluminum, Gangalee and Gurland observed that the fraction of broken silicon particles and particles debonded from the aluminum increased in proportion to the parameter $d^{1/2}/f^{1/3}$.

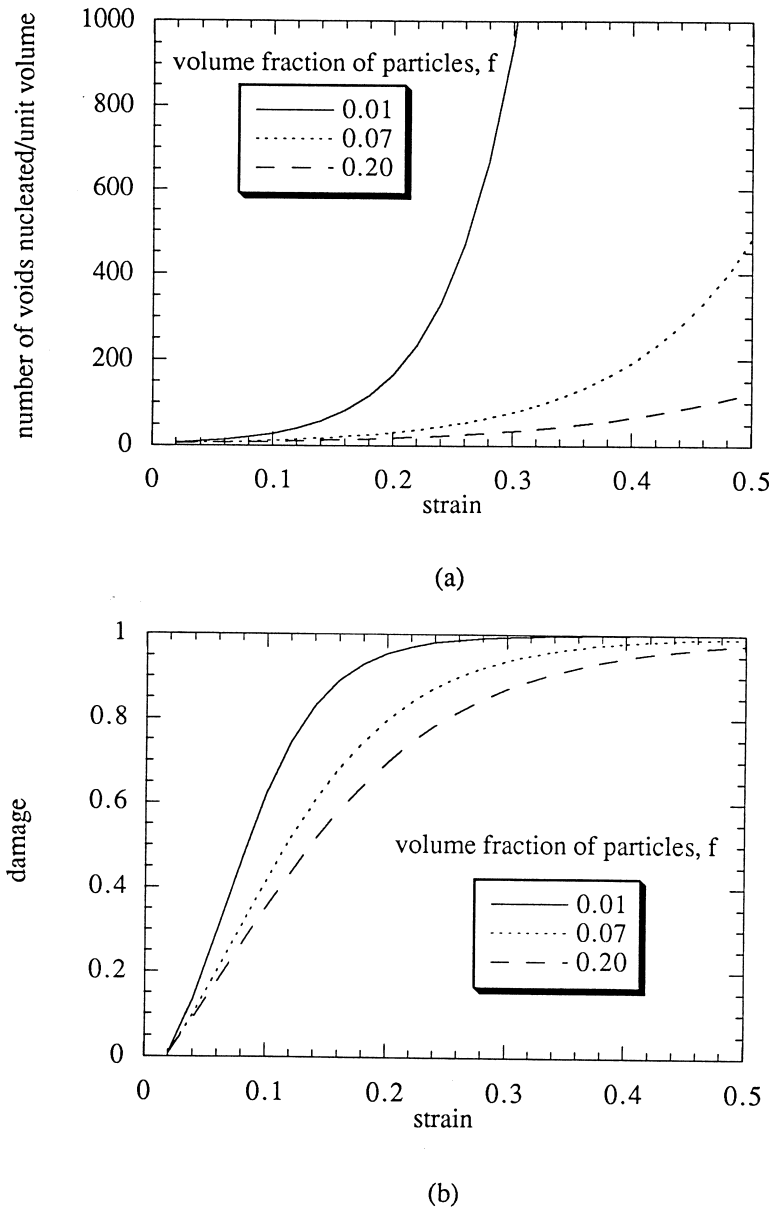

Fig. 4. (a) Nucleation per unit volume vs strain and (b) damage vs strain under uniaxial tension showing the decrease in number of voids and total damage as the particle volume fraction increases.

We have shown the trends related to the changes in the particle size, *d*. Now we show the trends for changes in the particle volume fraction. Figure 4(a) presents the number density of voids nucleated per unit volume vs strain level for increasing volume size. As the volume of second phase particles increases, the nucleation rate decreases. Similarly, Figure 4(b) shows the decreased

accumulation of total damage as the volume fraction increases. As expected, these trends follow closely with those of Gangalee and Gurland (1967).

4.3. *Fracture toughness*, K_{1C}

Spacing of particles is inherently incorporated into the nucleation evolution equation presented in eqn (14) in a phenomenological manner by employing the fracture toughness (Green and Knott, 1976; Rice and Johnson, 1970). This has been shown for small particles but not for large particles (Lee et al., 1985; Wojcieszynski, 1993). A range of fracture toughness is given here to illustrate the trends of the nucleation and damage rates. The fracture toughness for A356 cast aluminum ranges from 16.7–18.0 MPa-m**0.5 (Koh and Stephens, 1988), for titanium alloys (Ti–10V–2Fe–3Al, Ti–6Al–4V, and Ti–6Al–6V–2Sn) from 39.1–46.0 MPa-m***0.5, and for high purity 4340 steel up to 474 Mpa-m***0.5 (Cox and Low, 1974). Figure 5(a) shows the trends for nucleation when the fracture toughness is varied over the ranges listed above as a function of strain. Figure 5(b) shows the decreased accumulation of total damage as a function of strain as the fracture toughness increases. In these strain regimes, when the fracture toughness is fairly large (>46 MPa-m**0.5), nucleation occurs in a linear fashion with respect to strain but is more nonlinear as the fracture toughness decreases.

4.4. *Material constant*, C_{coeff}

The onset of nucleation can occur at various strains depending on the material. The material constant C_{coeff} is used to reflect this initial nucleation strain. It is essentially used to linearly scale the void nucleation equation to cover a wide range of materials. Figure 6 shows the trends for the void nucleation rate and damage rate as functions of strain. Note in Fig. 6(b) the different types of nonlinearities that can be modeled for damage when C_{coeff} is changed an order of magnitude.

4.5. *Stress state*

The motivation for including the stress invariants in eqn (14) is to allow for the void nucleation model to account for other stress states besides tension. The three deviatoric stress invariants used in eqn (14) have been used as yield 'type' functions before. Perzyna (1985) has introduced a general constitutive framework that uses a viscoplastic flow rule three invariants of overstress and a failure criterion. Before this, McClintock (1968); Rice and Tracey (1969); Gurson (1977a, b); Rousselier (1981); Tvergaard (1981; 1982a, b); Becker and Needleman (1986); Kim and Carroll (1987); Lee (1988); Cocks (1989); Mear (1990); Eftis and Nemes (1991); and Lee (1991) included the first two invariants in the yield function to analyze metallic behavior. Rudnicki and Rice (1975) used the first two invariants in determining localization effects in pressure-sensitive materials. Dorris and Nemat-Nasser (1980) and Nemat-Nasser and Shokooh (1980) used the first two invariants with isotropic hardening for compressible frictional geomaterials.

Edelman (1950) showed that the three independent stress invariants I_1, J_2, and J_3 represent a minimal integrity basis for a yield criterion. Adding J_3 has had some practical advantages in material modeling. Goldman et al. (1983) used J_3 in the yield function for determining the strength of polymers. Weng (1987) developed a micromechanical theory for high temperature creep of

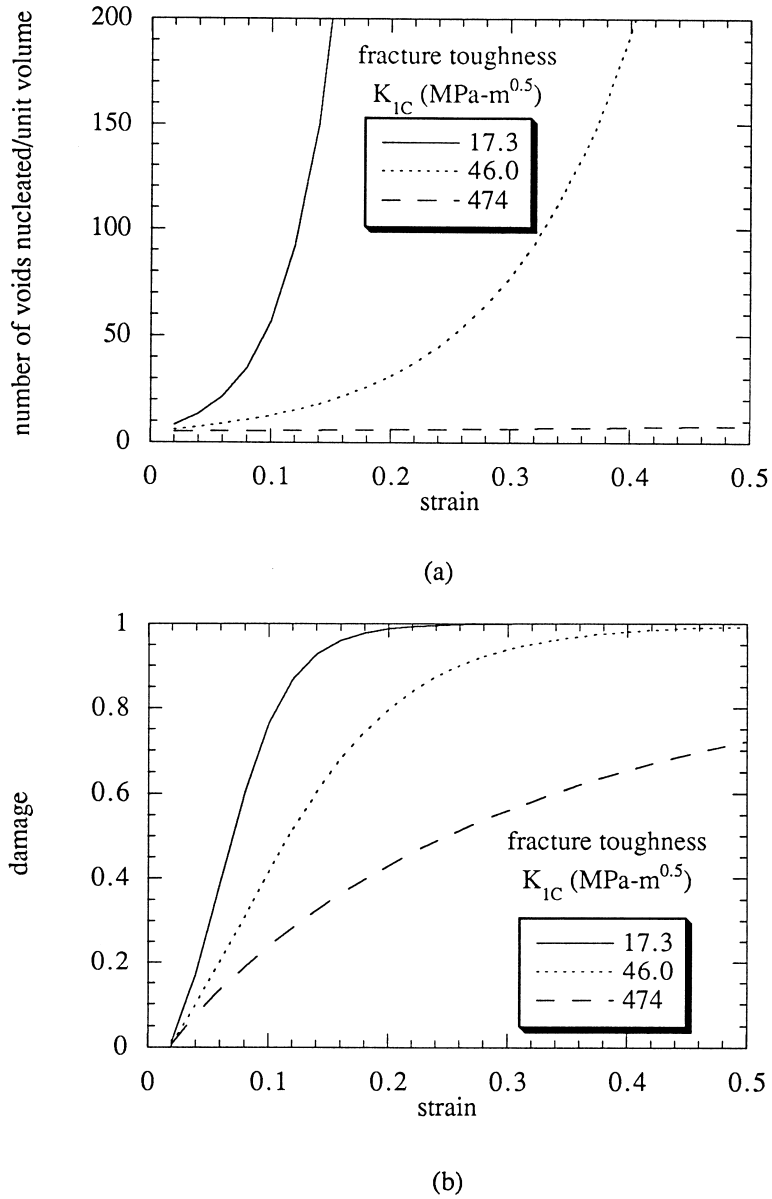

Fig. 5. (a) Nucleation per unit volume vs strain and (b) damage vs strain under uniaxial tension showing the decrease in number of voids and total damage as the fracture toughness increases.

polycrystals that included J_3 in the yield function and showed that the climb force weakly depended on J_3. Takeda et al. (1987) showed by experiments on thin-walled cylindrical specimens of a fully annealed mild steel under combined loadings of tension, internal pressure and torsion that the effect of J_3 on the yield behavior of material was larger than that of initial anisotropy. Papadopoulos

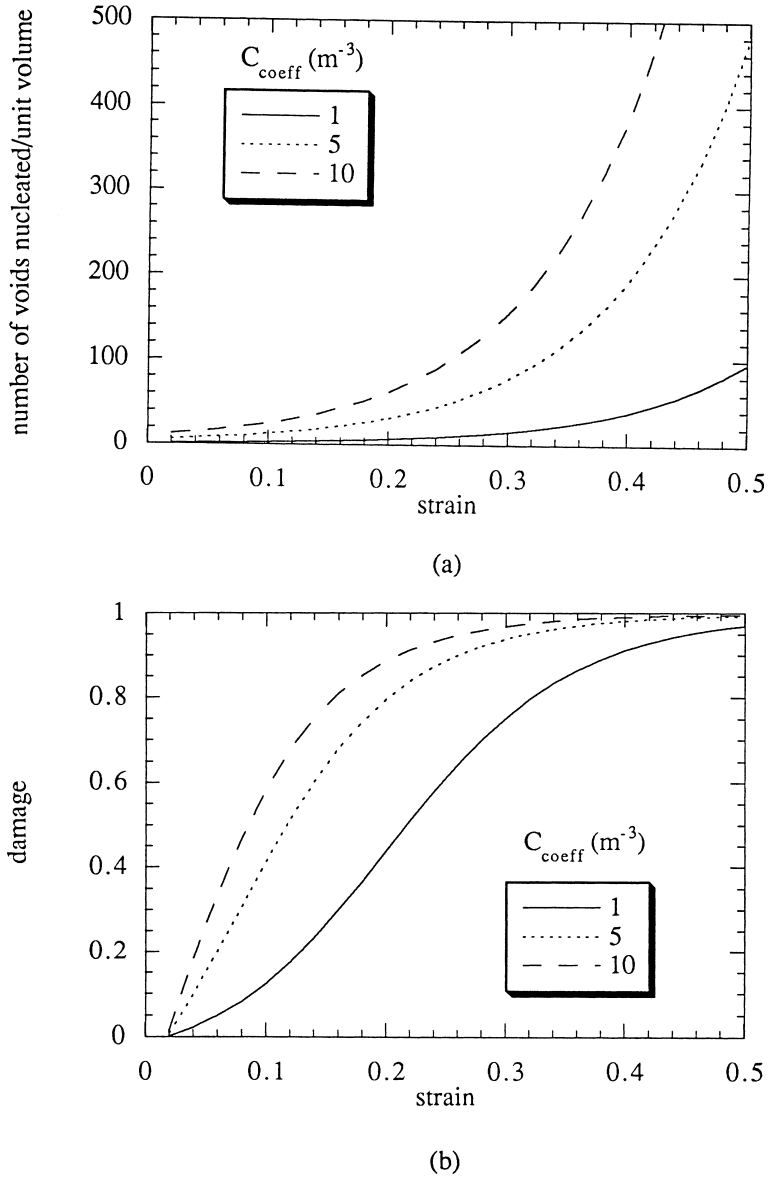

Fig. 6. (a) Nucleation per unit volume vs strain and (b) damage vs strain under uniaxial tension showing the decrease in number of voids and total damage as the coefficient constant increases.

(1988; 1989) employed J_3 to determine the crack propagation direction in polycrystalline metals. Kearsley (1989) showed the stretch effects within a single cube of using the three invariants. Gupta (1989) generalized Drucker's (1949) inclusion of J_3 into the yield function as a series function. Ohtaki (1988) used a seventh-degree yield function containing J_3 in a two dimensional finite element method for elasto-plasticity to get yield surfaces other than the von Mises yield function.

Over the years, J_3 has been included for modeling certain geomaterials by Desai et al. (1984; 1986), for sand by Poorooshasb (1989), and for concrete and soils by Schreyer (1984). Schreyer (1983a; b) also used J_3 to examine strain hardening, strain softening, dilatation, and compaction for frictional materials. De Boer and Dresenkamp (1989) used the three invariants with a non-associative flow rule to determine failure in concrete. Simo and Meschke (1993) added the first invariant to Desai et al.'s (1986) formulation along with the second and third invariants to arrive at new computational algorithms for finite strain plasticity but the approach was limited to rate independent, isotropic behavior.

Miller and McDowell (1992) were the first to employ stress invariants in internal state variable hardening equations. Drucker (1949) explained that J_3 enabled the proper weighting of the shearing stresses acting on the various slip planes. Miller and McDowell (1992) asserted that J_3 reflects a change of constraint on slip as a function of stress state and thus should be used in the hardening equations in addition to the yield function. Horstemeyer et al. (1995) slightly modified the Miller and McDowell (1992) form of the hardening equations of Bammann (1988) to illustrate localization and shear bands related to forming limits.

To the authors' knowledge, employing the three stress invariants to distinguish various stress states has not been applied to modeling void nucleation. Hence, eqn (9) allows nucleation to be a function of stress triaxiality and also distinguishes between tension, compression, and torsion.

The material constants a, b, and c in eqn (9) relate to the volume fraction of nucleation events arising from local microstresses in the material and as such have dimensions of stress (MPa). These constants are determined experimentally from compression, torsion, and tension tests whereby the density of voids nucleated is measured at different strain levels.

The use of stress invariants in nondimensional form as shown in eqn (14) allows for robust determination of the nucleation constants from the various stress state effects. If a, b, and c are zero, the damage evolution form of eqn (3) reduces to just void growth. In torsion, the constant a is determined. The constants b and c are determined from tension and compression tests. For future reference, the constant a is referred to as the torsional constant, b as the tension/compression constant, and c as the triaxiality constant. Table 2 shows the delineation of effects from the stress state dependence.

Table 2
The stress invariant expressions under different stress states

	Tension	Compresion	Torsion
$\frac{4}{27}-\frac{J_3^2}{J_2^3}$	0	0	$\frac{4}{27}$
$\frac{J_3}{J_2^{3/2}}$	$\frac{2}{3\sqrt{3}}$	$-\frac{2}{3\sqrt{3}}$	0
$\lVert\frac{I_1}{J_2^{1/2}}\rVert$	1	1	0

4.5.1. Stress triaxiality constant, c

The influence of the stress triaxiality has been observed for nucleation of voids related to second phases in the works of Cox and Low (1974) and French and Weinrich (1974). Park and Thompson (1988) for 1520 steel, observed that voids started at both sides of the tensile pole of the particle. Because tensile states exist for even compression loadings, some nucleation events are expected to occur even under compression loads. The model allows for this capability. Figure 7(a) and (b) show the increase in density of voids nucleated per unit volume and damage, respectively, as a function of strain for an increase in the triaxiality constant, c.

4.5.2. Tension/compression constant, b

Figure 8(a) and (b) show the increase in voids nucleated per unit volume and damage, respectively, as a function of strain for an increase in the tension/compression constant, b. Note that the trends are nonlinear in a similar manner as when the triaxiality constant, c, is used. Also, note that nucleation occurs more rapidly in tension than compression which concurs with intuition.

4.5.3. Torsional constant, a

Figure 9(a) and (b) shows the increase in voids nucleated per unit volume and damage, respectively, as a function of strain for an increase in the torsional constant, a. Figure 9 illustrates that much more torsional straining is needed to achieve the same amount of damage as under tension. This arises because the void growth is based on the stress triaxiality which is zero for torsion. Hence the damage purely accumulates due to nucleation events.

4.5.4. Multiaxial responses

The void nucleation model can be used for multiaxial stress states as shown in Fig. 10. The nucleation model parameters were chosen such that the lowest void nucleation rate arises for simple shear (torsion) and the next lower rate arises for compression. The upper limit of void nucleation occurs when the multiaxial condition of tension plus torsion is applied giving just a slightly higher nucleation rate than tension alone. The constants in Table 1 were employed for illustrative purposes, but different values for the constants would obviously place a different level of influence from the stress site on the nucleation behavior. As such, any material can be accommodated given that experimental data is available.

Figure 10(b) shows the damage level vs strain for the same multiaxial loading conditions in Fig. 10(a). In these calculations the initial porosity level was assumed to be 0.001. The damage trends are different than the nucleation trends because of the stress state dependence on the void growth rule (eqn 15). Void growth would dominate over void nucleation when tensile triaxialities are present. Under compression and torsion, void growth is typically less.

5. Model compared to experimental data

Several examples are presented in which the void nucleation model constants are determined from tension data in the literature and from a cast Al–Si–Mg aluminum alloy under various loading conditions.

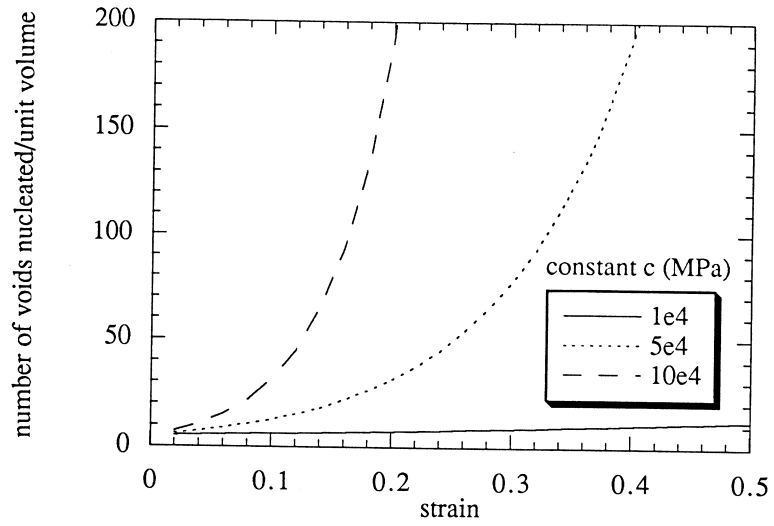

(a)

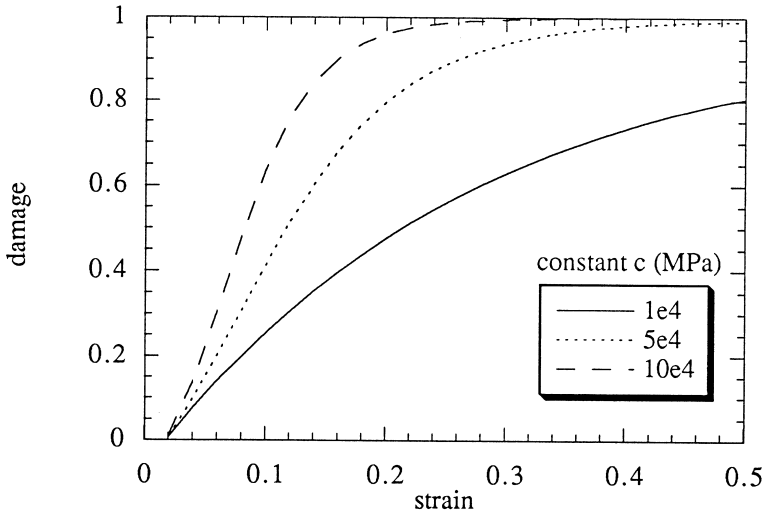

(b)

Fig. 7. (a) Nucleation per unit volume vs strain and (b) damage vs strain under uniaxial tension showing the increase in number of voids and total damage as the triaxiality constant, c, increases.

5.1. Nucleation model correlation to literature data

Cox and Low (1974) experimentally determined void nucleation data as a function of strain for a commercial grade and high purity grade of AISI 4340 steel. The commercial grade had essentially a higher diameter size of inclusion on average. A silicon–aluminum alloy was analyzed by Fisher

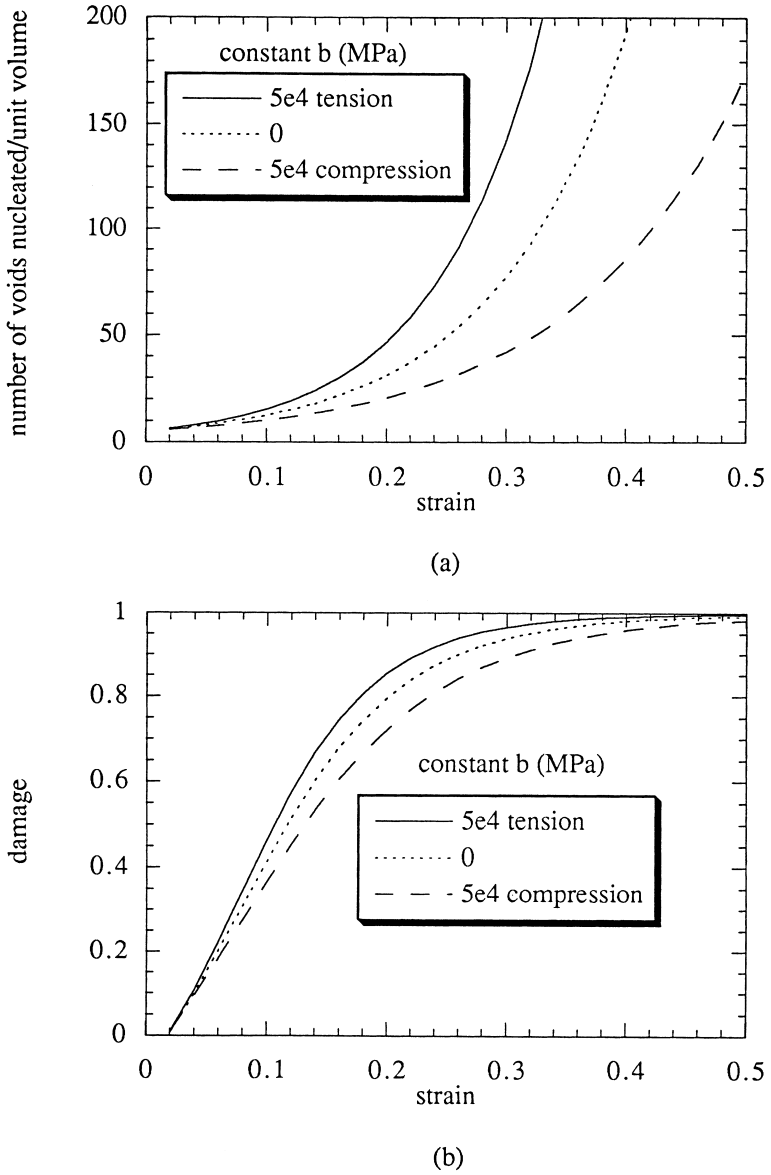

Fig. 8. (a) Nucleation per unit volume vs strain and (b) damage vs strain showing the change in number of voids and total damage as the tension/compression constant, b, changes.

and Gurland (1981a) for void nucleation. This nucleation data was chosen for our study because of its different yield, plasticity, and fracture characteristics. Finally, Maloney and Garrison (1989) analyzed a HY180 steel for void nucleation. In their study, the second phase was changed from MnS to Ti_2CS to understand the effects on fracture. Table 3 summarizes the values for the parameters and constants for each of the materials. Here the parameters are defined by the fracture

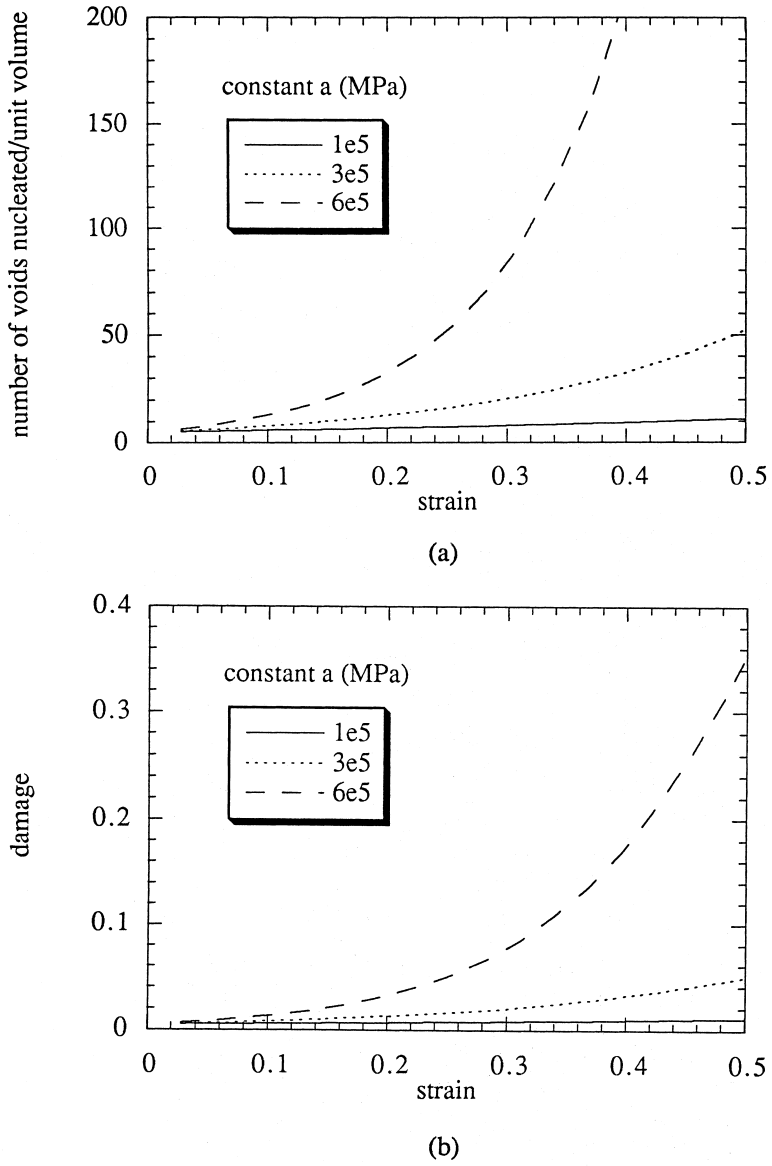

Fig. 9. (a) Nucleation per unit volume vs strain and (b) damage vs strain under torsion showing the increase in number of voids and total damage as the torsional constant, a, increases.

toughness, length scale parameter (in these correlations the average particle size was chosen as the length scale parameter), and inclusion volume fraction. The material constants are denoted by C_{coeff}, a, b, and c.

Figure 11 shows the correlation of the model to the Cox and Low (1974) data. In the determination of the material constants, C_{coeff} was different by an order of magnitude. This illustrates

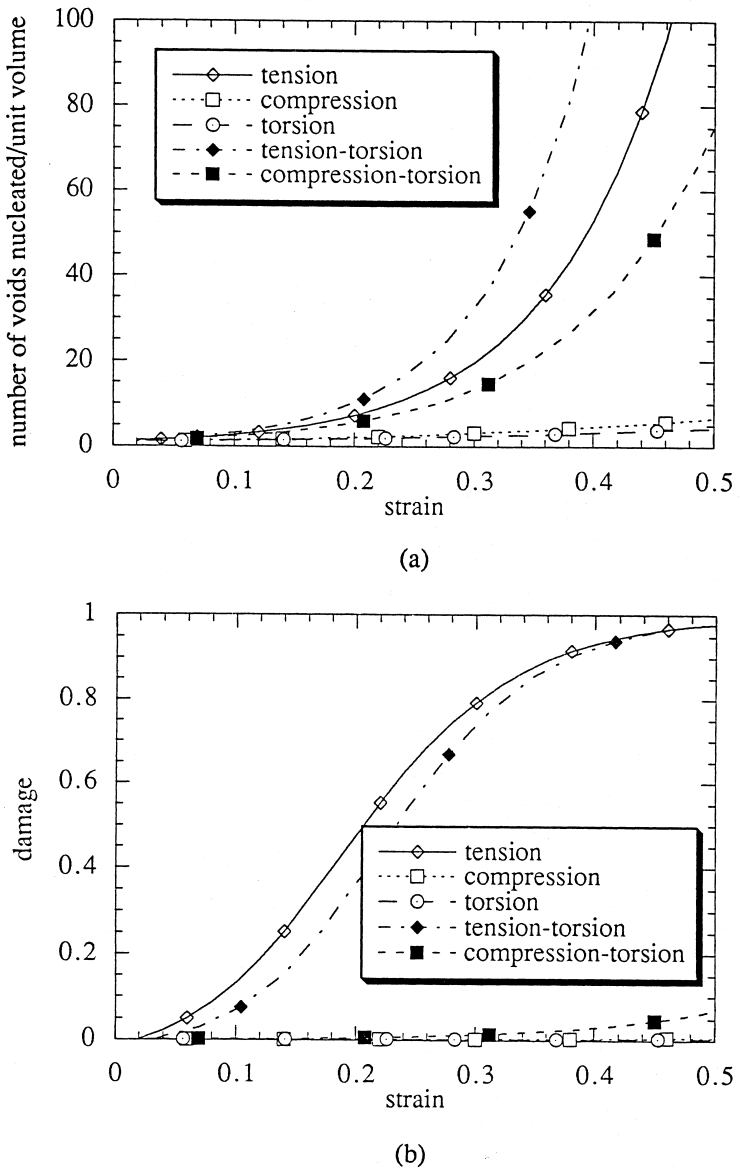

Fig. 10. (a) Nucleation per unit volume vs strain and (b) damage vs strain under various loading conditions.

the increase in voids nucleating from larger second phase particles. Constants a and b were chosen to be zero because torsion and compression data were not available. Since the fracture toughness, average inclusion size, and inclusion volume fraction were different in both types of 4340 steel, one might expect that the constant c would be the same for both types. The constant c did not indeed need change. Hence, the average size of the inclusions, the fracture toughness, and inclusion volume fraction can account for the local stress state affecting void nucleation in these 4340 steels.

Table 3
The constants and parameters determined from various literature data

Parameters	Cox and Low (1974)—small d	Cox and Low (1974)—large d	Fisher and Gurland (1981a)	Maloney and Garrison (1989)—MnS	Maloney and Garrison (1989)—Ti_2CS
d (μm)	4.5	9.7	14	16	10
f	0.06	0.06	0.066	0.00021	0.00019
K_{IC} (MPa-m**0.5)	106.8	74.6	219.8	254	474
C_{coeff}	0.922	10.6	0.025	1.09e-4	6.55e-7
a (MPa)	0	0	0	0	0
b (MPa)	0	0	0	0	0
c (MPa)	9.78e4	9.78e4	10.59e4	5.55e4	26.4e4

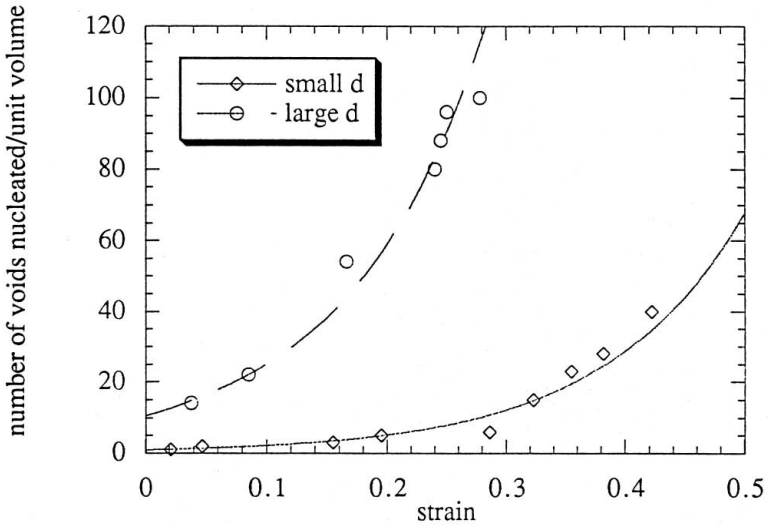

Fig. 11. Nucleation per unit volume vs strain comparing the model and experimental data of 4340 steel from Cox and Low (1974). The dots represent the experimental data, and lines display the model results. The larger average inclusion size ($d = 9.7$ μm) shows a higher void nucleation rate than the smaller average inclusion size ($d = 4.5$ μm).

Figure 12 shows the correlation of the model to the Fisher and Gurland (1981) data. Interestingly, the value for the constant c was near that of 4340 steel (about a 10% difference). This may be due to the local mechanical properties of the second phase of the silicon–aluminum is similar to that of the 4340 steel. The value for C_{coeff} was less than that for 4340 steel.

Figure 13 shows the correlation of the model to the Maloney and Garrison (1989) silicon–aluminum data. The MnS inclusions embedded within the HY180 steel had a higher void nucleation rate than the Ti_2CS inclusions. This occurred because of the slightly higher average size and also

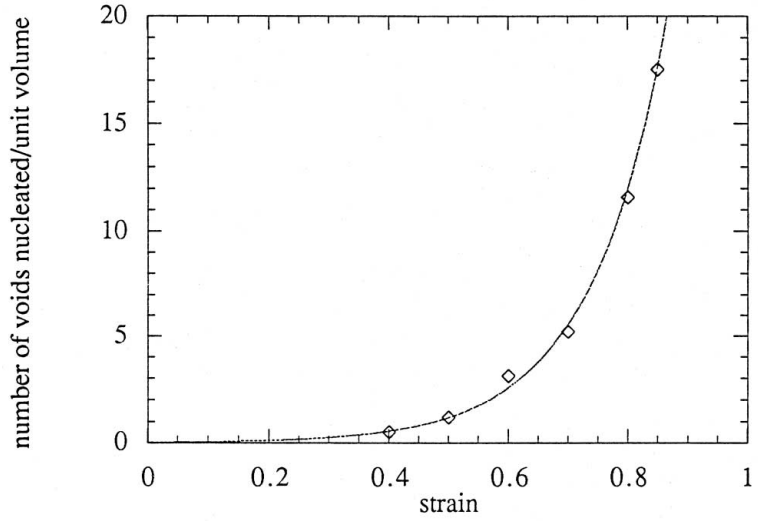

Fig. 12. Nucleation per unit volume vs strain comparing the model and experimental data of silicon–aluminum from Fisher and Gurland (1981a). The dots represent the experimental data, and lines display the model results.

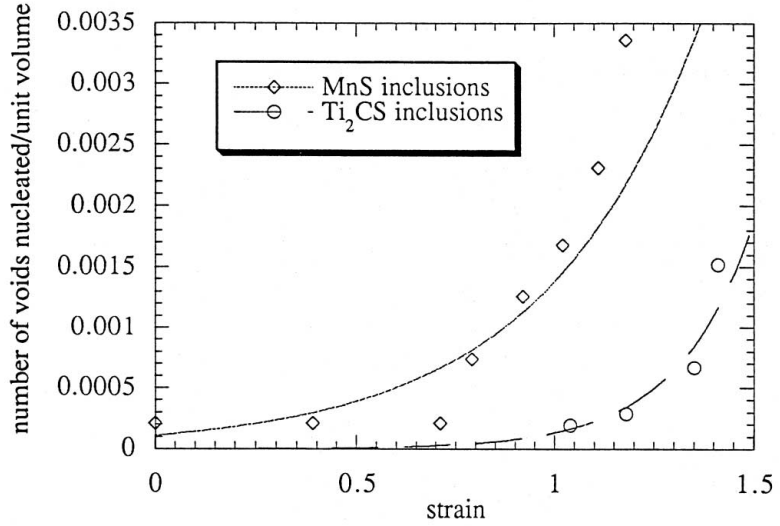

Fig. 13. Nucleation per unit volume vs strain comparing the model and experimental data of HY180 steel with two different main second phase inclusions from Maloney and Garrison (1989). The dots represent the experimental data, and lines display the model results.

because of the decreased fracture toughness. The value for C_{coeff} was much less for the HY steels than for the aluminum because the void nucleation rate was much lower.

One might think that the constant c should not change for both types of HY180 steel considering

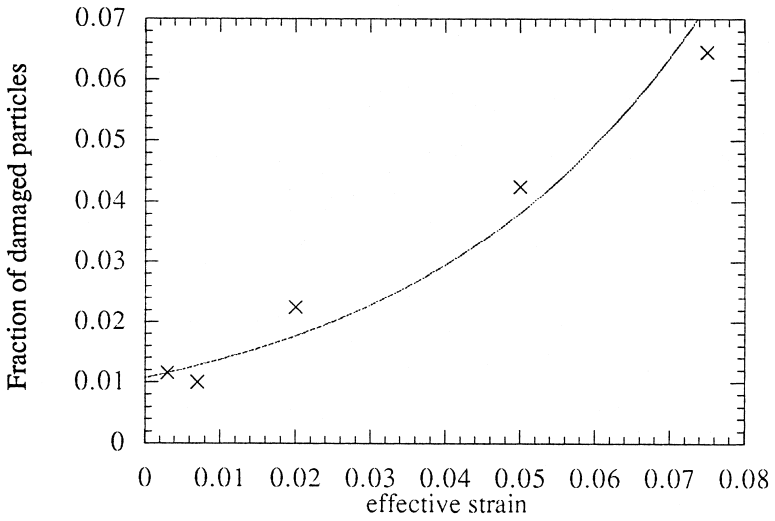

Fig. 14. Comparison of void nucleation model with cast Al–Si–Mg aluminum alloy data in tension.

the arguments for the 4340 steel with two different average inclusion sizes. However, the model correlation to the data reveals that the constant c was different for the two types of HY180 steel. One explanation might be that the inclusion material for 4340 steel was identical, but the inclusion material for the HY180 steel was different. This difference in material properties would locally affect the stress state that drives void nucleation. Note also that C_{coeff} is different as well for the two types of HY180 steel.

5.2. Nucleation model correlation under different load conditions

The previous examples were performed under uniaxial tension. One key contribution of this void nucleation model is the stress state dependence. Tests were performed to give insight into the stress state dependence of void nucleation under tension, compression, and torsion. The tests were stopped at various effective strain levels, and the specimens were cut, polished, and examined for void nucleation. The accumulation of new voids occurred by fracture of the second phase silicon and by debonding of the silicon with the aluminum. The void nucleation sites were counted over a statistically significant region of the material at the different strain levels, and then the void nucleation model constants were determined. The experiments are discussed in more detail in a forthcoming paper (Horstemeyer et al., 1998).

Figures 14–16 show the fraction of damaged particles vs strain for the model and experimental data under tension, compression, and torsion, respectively. The fraction of damaged particles is defined as the void nucleation density divided by the total number of silicon particles. Under tension, both silicon fracture and interfacial debonding occurred, but under compression and torsion only silicon fracture occurred. For Figs 14 and 15, the void nucleation model constants b and c were determined to be 5.86e4 and 5.20e4 MPa, respectively. For Fig. 16, the torsional

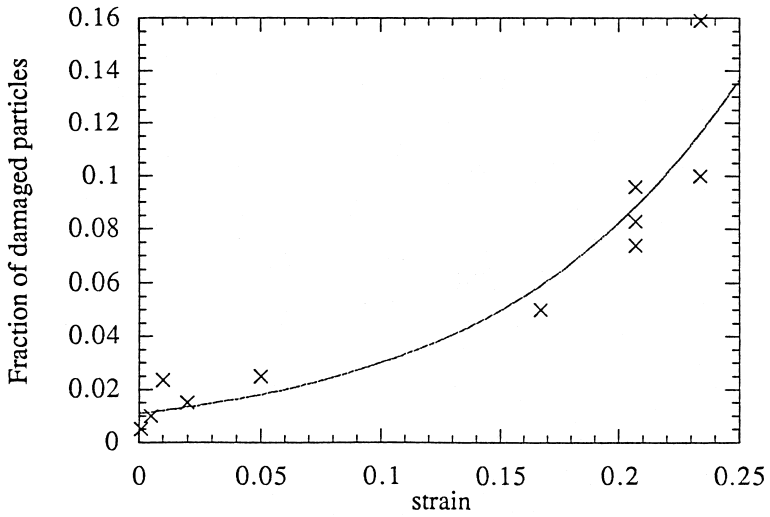

Fig. 15. Comparison of void nucleation model with cast Al–Si–Mg aluminum alloy data in compression.

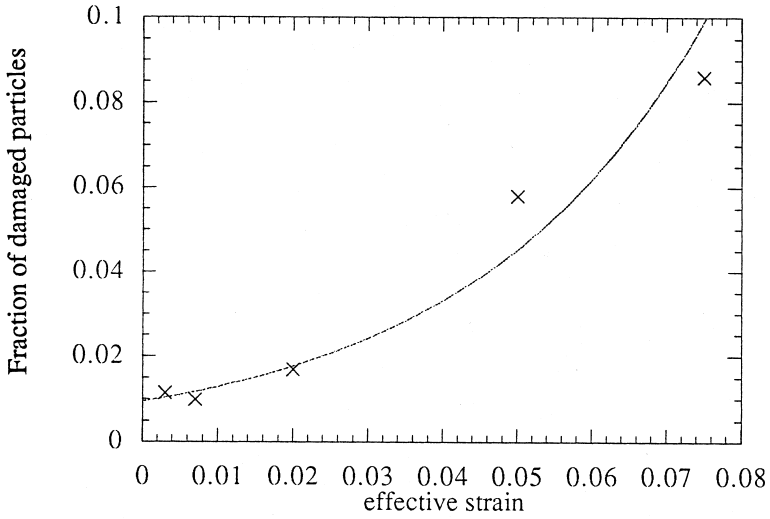

Fig. 16. Comparison of void nucleation model with cast Al–Si–Mg aluminum alloy data in torsion.

constant a was 6.16e5 MPa. For the three cases, C_{coeff} was 0.01. These parameters are summarized in Table 4.

6. Closure

A void nucleation evolution model is presented that is a function the fracture toughness of the aggregate material, a length scale parameter (taken to be the average size of the second phase

Table 4
The parameters for a cast Al–Si–Mg alloy under various loading conditions

Parameters	Multiaxial values
d (μm)	8
f	0.07
K_{IC} (MPa-m**0.5)	17.3
C_{coeff}	0.01
a (MPa)	6.16e5
b (MPa)	5.86e4
c (MPa)	5.20e4

particles in the examples shown in this writing), the volume fraction of the second phase, strain rate, and stress state. The parametric trends are illustrated and model constants and parameters are shown for several materials from literature data. Different loading tests were performed for this study for a cast Al–Si–Mg aluminum alloy to analyze the stress state dependence of void nucleation. The void nucleation model was then correlated to the multiaxial void nucleation data.

Acknowledgements

The authors are greatly indebted to Douglas J. Bammann, Dan Mosher, and Lee Davison for discussions about the damage framework. Warren Garrison is also to be thanked for the many helpful discussions about nucleation of voids in ductile materials. The support and interest of Richard Osborne is also appreciated. This work has been sponsored by the U.S. Department of Energy, Sandia National Laboratories under contract DE-AC04-94AL85000.

References

Argon, A.S., Im, J., Safoglu, R., 1975. Cavity formation from inclusions in ductile fracture. Metall. Trans. 6A, 825–837.

Asaro, R.J., 1979. Geometrical effects in the inhomogeneous deformation of ductile single crystals. Acta Metall. 27, 445.

Ashby, M., 1966. Work hardening of dispersion-hardened crystals. Phil. Mag. 14, 1157–1178.

Avrami, M., 1939. Kinetics of phase change. J. Chem. Phys. 7, 1103–1112.

Bammann, D.J., 1988. Modelling the large strain-high temperature response of metals. In: Giamei, A.F., Abbaschian, G.J. (Eds), Modelling and Control of Casting and Welding Processes IV, TMS Publications, Warrendale, PA.

Barbee, T.W., Seaman, L., Crewdson, R., Curran, D., 1972. Dynamic fracture criteria for ductile and brittle metals. J. Materials JMLSA 7 (3), 393–401.

Becker, R.C., Needleman, A., 1986. Effect of yield surface curvature on necking and failure in porous plastic solids. ASME J. Applied Mech. 53, 491–499.

Brickstad, B., 1983. A viscoplastic analysis of rapid crack propagation experiments in steel. J. Mech. Phys. of Solids 31, 307–327.

Chen, E.P., Kipp, M.E., Grady, D.E., 1984. A strain-rate sensitive rock fragmentation model. In: Chong, K.P., Ward Smith J. (Eds.), Mechanics of Oil Shale, Elsevier Applied Science Publishers, NY, pp. 423–456.
Cocks, A.C.F., 1989. Inelastic deformation of porous materials. J. Mech. Phys. Solids 37 (6), 693–715.
Coleman, B.D., Gurtin, M.E., 1967. Thermodynamics with internal state variables. J. Chem. Phys. 47, 597.
Cox, T.B., Low, J.R. Jr, 1974. An investigation of the plastic fracture of AISI 4340 and 18 Nickel-200 Grade Maraging Steels. Metall. Trans. 5, 1457–1470.
Davison, L., Stevens, A.K., Kipp, M.E., 1977. Theory of spall damage accumulation in ductile metals. J. Mech. Phys. Solids 25, 11–28.
De Boer, R., Dresenkamp, H.T., 1989. Constitutive equations for concrete in failure state. J. Eng. Mech. 115 (8) 1591–1608.
Desai, C.S., Siriwardane, H.J., 1984. Constitutive Laws for Engineering Materials with Emphasis on Geologic Materials, Prentice-Hall, Inc., Englewood Cliffs, NJ.
Desai, C.S., Somasundaram, S., Frantziskonis, G., 1986. A hierarchical approach for constitutive modeling of geologic materials. Int. J. Num. Methods Eng. 10, 225–257.
Dorris, J.F., Nemat-Nasser, S., 1980. A plasticity model for flow of granular materials under triaxial stress states. Int. J. Solids Structures 18 (6), 497–531.
Drucker, D.C., 1949. Stress-strain relations for strain hardening materials: discussion and proposed experiments. Proc. Symposia Appl. Math., Vol. 1, p. 181.
Edelman, F., 1950. On the Coincidence of Plasticity Solutions Obtained with Incremental and Deformation Theories. Ph.D. thesis, Brown University.
Eftis, J., Nemes, J.A., 1991. Evolution equation for the void volume growth rate in a viscoplastic-damage constitutive model. Int. J. Plasticity 7, 275–293.
Fisher, J.R., Gurland, J., 1981. Void nucleation in spheroidized carbon steels part 1: Experimental. Metal Science 185–192.
French, I.E., Weinrich, D.F., 1974. The influence of hydrostatic pressure on the tensile deformation of a spheroidized 0.5%C steel. Scripta Metall. 8, 87.
Gangalee, A., Gurland, J., 1967. On the fracture of silicon particles in aluminum-silicon alloys. Trans. Metall. Soc. of AIME 239, 269–272.
Garrison, W.M. Jr, 1986. The effect of silicon and nickel additions on the sulfide spacing and fracture toughness of a 0.4 carbon low alloy steel. Metall. Trans. A 17A, 669–678.
Goldman, A.Y., Freidin, A.B., Lebedev, A.A., 1983. Dependence of the yield point of polymer materials on hydrostatic pressure and certain plasticity criteria. Journal of Problemy Prochnosti 15 (3), 62–66.
Goods, S.H., Brown, L.M., 1979. The nucleation of cavities by plastic deformation. Acta Metall. 27, 1–15.
Green, G., Knott, J.F., 1976. The initiation and propagation of ductile fracture in low strength steels. J. Eng. Mater. Tech. ASME, Fairfield, NJ, 98, 37–46.
Gupta, N.K., 1989. A description of experimental yield surfaces. Proc. Plasticity 1989, Second Int. Symp. Plasticity, Pergamom Press, Oxford-NY, pp. 91–94.
Gurland, J., Plateau, J., 1963. The mechanism of ductile rupture of metals containing inclusions. Trans. ASM 56, 442.
Gurland, J., 1972. Observations on the fracture of cementite particles in a spheroidized 1.05%C steel deformed at room temperature. Acta Metall. 20, 735–741.
Gurson, A.L., 1977a. Continuum theory of ductile rupture by void nucleation and growth-1. Yield criteria and flow rules for porous ductile media. J. Engng. Materials Techn. 99, 2–15.
Gurson, A.L., 1997b. Porous rigid-plastic materials containing rigid inclusions-yield function, plastic potential, and void nucleation. Proc. Int. Conf. Fracture, D.M.R. Taplin (Ed.), 2A, 357–364.
Gysler, A., Lutjering, G., Gerold, V., 1974. Deformation behavior of age-hardened Ti-Mo alloys. Acta Metall. 22, 901.
Hahn, G.T, Kanninen, M.F., Rosenfield, A.R., 1968. Fracture toughness of materials. A. Rev. Mater. Sci. 2, 381.
Hahn, G.T., Rosenfield, A.R., 1975. Metallurgical factors affecting fracture toughness of aluminum alloys. Metall. Trans. A 6A, 653–668.
Hirth, J.P., Nix, W.D., 1985. Analysis of cavity nucleation in solids subjected to external and internal stresses. Acta Metall. Mater. 33, 359.
Horstemeyer, M.F., Lathrop, J., Gokhale, A.M., Dighe, M., 1998. Modeling stress state dependent damage evolution in a cast Al–Si–Mg aluminum alloy. in press.

Horstemeyer, M.F., McDowell, D.L., Bammann, D.J., 1995. Torsional softening and the forming limit diagram. SAE Tech. Ser. 960599, K. Chen (Ed.). Analysis of Autobody Stamping Technology.

Irwin, G.R., 1958. Fracture I. Handbuch der Physik VI, Flugge (Ed.), Springer, pp. 558–590.

Kanninen, M.F., Popelar, C.H., 1985. Advanced Fracture Mechanics, Oxford Univ. Press.

Kearsley, E.A., 1989. Strain invariants expressed as average stretches. Journal of Rheology 33 (5), 757–760.

Kim, K.T., Carroll, M.M., 1987. Compaction equations for strain-hardening porous materials. Int. J. Plasticity 3, 63–73.

Koh, S.K., Stephens, R.I., 1988. Fracture toughness of A356-T6 cast aluminum. SAE-SP760, Fatigue and Fracture Toughness of A356-T6 Cast Aluminum Alloy, 881705, pp. 61–69.

Leblond, J.B., Perrin, G., Devaux, J., 1995. An improved Gurson-type model for hardenable ductile metals. European J. of Mechanics A, Solids 14 (4), 499–527.

Lee, Y.K., 1988. A finite elastoplastic flow theory for porous media. Int. J. Plasticity 4, 301–316.

Lee, Y.S., 1991. Modeling Ductile Damage Evolution in Metal Forming Processes. Ph.D. Thesis, Mechanical Engineering, Cornell University, Ithaca, NY.

Lee, S., Majno, L., Asaro, R.J., 1985. Correlation of microstructure and fracture toughness in two 4340 steels. Metall. Trans. A 16A, 1633–1648.

Lu, W.Y., Horstemeyer, M.F., Korellis, J.S., Grishabar, R.B., Mosher, D., 1997. High temperature notch sensitivity of AISI 304L stainless steel. Submitted to JEMT.

Maloney, J.L., Garrison, W.M. Jr, 1989. Comparison of void nucleation and growth at MnS and Ti_2CS inclusions in HY180 steel. Scripta Metall. 23, 2097–2100.

Marin, E., 1993. A Critical Study of Finite Strain Porous Inelasticity. PhD Thesis, Georgia Institute of Technology.

McClintock, F.A., 1968. A criterion for ductile fracture by the growth of holes. ASME J. Appl. Mech. 35, 363.

McDowell, D.L., Marin, E., Lee, Y.K., Miller, M.P., Bertoncelli, C., 1992. Considerations for a 'complete' continuum theory of multiaxial inelasticity for ductile metals. MECAMAT'92 International Seminar on Multiaxial Plasticity, 1–4 September, Cachan, France.

Mear, M.E., 1990. On the plastic yielding of porous metals. Mech. Matls. 9, 33–48.

Miller, M.P., McDowell, D.L., 1992. Stress state dependence of finite strain inelasticity. ASME Summer Applied Mechanics Meeting, Tucson, AZ, ASME AMD-Vol 32, Microstructural Characterization in Constitutive Modeling of Metals and Granular Media, pp. 27–44.

Moody, N.R., Garrison, M. Jr, Smugeresky, J.E., Costa, J.E., 1993. The role of inclusion and pore content on the fracture toughness of powder-processed blended elemental titatium alloys. Metall. Trans. A 24A, 161–174.

Nemat-Nasser, S., Shokooh, A., 1980. On finite plastic flows of compressible materials with internal friction. Int. J. Solids Structures 16, 495–514.

Needleman, A., Rice J.R., 1978. Limits to ductility set by plastic flow localization. In: Koistinen, D.P., Wang, N.M. (Eds). Mechanics of Sheet Metal Forming, Plenum Publishing Co., pp. 237–265.

Nieh T.G., Nix, W. D., 1980. A comparison of the dimple spacing on intergranular creep fracture surfaces with the slip band spacing for copper. Scripta Metall. 14, 365.

Ohtaki, S., 1988. An analysis of the two-dimensional elasti-plastic stress problem using quadratic programming: the case of adopting the seventh-degree yield function containing the third invariant of the deviatoric stress tensor. Nippon Kikai Cakkai Ronbunshui 54 (502).

Palmer, I.G., Smith, G.C., 1967. Fracture of internally oxidized copper alloys. Proc. AIME Conf. Oxide Dispersion Strengthening, Bolton Landing, NY, June 1966. Gordan & Beach, NY.

Park, I.G., Thompson, A.W., 1988. Ductile fracture in spheroidized 1520 steel. Acta Metall. 36, 1653–1664.

Papadopoulos, G.A., 1988. Dynamic crack-bifurcation by the det-criterion. Engineering Fracture Mechanics 31 (5), 887–893.

Papadopoulos, G,.A., Ponridis, P.I., 1989. Crack initiation under biaxial loading with higher-order approximation. Engineering Fracture Mechanics 32 (3), 351–360.

Perzyna, P., 1985. Constitutive modeling of dissipative solids for postcritical behavior and fracture. ASME J. Engr. Mater. Tech. 106, 410–419.

Poorooshasb, H.B., 1989. Description of flow of sand using state parameters. Computers and Geotechnics 8, 195–218.

Puttick, K.E., 1959. Ductile fracture in metals. Phil. Mag. 4, 964.

Raj, R., Ashby, M.F., 1975. Intergranular fracture at elevated temperature. Acta Metall. Mater. 23, 653.

Rice, J.R., Tracey, D.M., 1969. On the ductile enlargement of voids in triaxial stress fields. J. Mech., Phys. Solids 17, 201.

Rice, J.R., Johnson, M.A., 1970. The role of large crack tip geometry changes in plane strain fracture. In: Kanninen, M.F., Adler, W.G., Rosenfield, A.R., Jaffee, R.J. (Eds). McGraw-Hill, New York, NY, pp. 641–672.

Rosenfield, A.R., 1968. Criteria for ductile fracture of two-phase alloys. Metall. Rev. 13, 29–40.

Rousselier, G., 1981. Finite deformation constitutive relation including ductile fracture damage. In: Nemat-Nasser, S. (Ed.), Three Dimensional Constitutive Relations and Ductile Fracture, North Holland Publ., pp. 331–355.

Rudnicki, J.W., Rice, J.R., 1975. Conditions for localization of deformation in pressure-sensitive dilatant materials. J. Mech. Phys. Solids 23, 371–394.

Saje, M., Pan, J., Needleman, A., 1982. Void nucleation effects on shear localization in porous plastic solids. Int. J. Fracture 19, 163–182.

Schreyer, H.L., Bean, J.E., 1983a. A simplified viscoplastic theory for frictional materials. Symp. Proc. U.S. Air Force Academy, Colorado, AD-A132 115, 77–80.

Schreyer, H.L., 1983b. A third-invariant plasticity theory for frictional materials. Journal of Structural Mechanics 11 (2), 177–96.

Schreyer, H.L., 1984. Development of a Third-Invariant Plasticity Theory for Concrete and Soils, Final Report, AFWL-TR-83-119, February.

Simo, J.C., Meschke, G., 1993. A new class of algorithms for classical plasticity extended to finite strains: Applications to geomaterials. Computational Mechanics, Vol 11, Springer-Verlag, pp. 253–278.

Takeda, T., Kikuchi, S., Nasu, Y., 1987. Experimental evaluation of yield condition containing third invariant of deviatoric stresses. Proceedings of the Thirtieth Japan Congress on Materials Research, pp. 13–18.

Tvergaard, V., 1981. Influence of voids on shear band instability under plane strain conditions. Int. J. Frac. 17 (4), 389–407.

Tvergaard, V., 1982a. Ductile fracture by cavity nucleation between larger voids. J. Mech. Phys. Solids 30, 265–286.

Tvergaard, V., 1982b. On localization in ductile materials constaining spherical voids. Int. J. Frac. 18, 237–252.

Tvergaard, V., 1990. Material failure by void growth to coalescence. In: Hutchinson, J.W., Wu, T.Y. (Eds). Advances in Applied Mechanics, Vol. 27, pp. 83–151.

Weng, G.J., 1987. Anisotropic hardening in single crystals and the plasticity of polycrystals. Int. J. Plast. 3, 315–339.

Wilsdorf, H.G.F., 1983. The ductile fracture of metals: A microstructural viewpoint. Mater. Sci. Engng. 59, 1.

Wojcieszynski, A., 1993. Particle Spacing and Grain Size Effects on Fracture Toughness, PhD Thesis, Carnegie Mellon University, Pittsburgh, PA.

Zhao, Y.H., Tandon, G.P., Weng, G.J., 1989. Elastic moduli for a class of porous materials. Acta Mechanica 76, 105–130.